Organic & Biomolecular Chemistry

PAPER

View Article Online
View Journal | View Issue

Cite this: *Org. Biomol. Chem.*, 2017, **15**, 4122

Exploring the reversal of enantioselectivity on a zinc-dependent alcohol dehydrogenase†

Miguel A. Maria-Solano, Adrian Romero-Rivera and Sílvia Osuna *

Received 26th February 2017,
Accepted 9th April 2017

DOI: 10.1039/c7ob00482f

rsc.li/obc

Alcohol Dehydrogenase (ADH) enzymes catalyse the reversible reduction of prochiral ketones to the corresponding alcohols. These enzymes present two differently shaped active site pockets, which dictate their substrate scope and selectivity. In this study, we computationally evaluate the effect of two commonly reported active site mutations (I86A, and W110T) on a secondary alcohol dehydrogenase from *Thermoanaerobacter brockii* (TbSADH) through Molecular Dynamics simulations. Our results indicate that the introduced mutations induce dramatic changes in the shape of the active site, but most importantly they impact the substrate–enzyme interactions. We demonstrate that the combination of Molecular Dynamics simulations with the tools POVME and NCIplot corresponds to a powerful strategy for rationalising and engineering the stereoselectivity of ADH variants.

1. Introduction

Biocatalysis is based on the application of natural catalysts for new purposes, for which the enzymes were not designed. The advantages of biocatalysts with respect to traditional catalysts make enzyme-based routes a preferable alternative for the synthesis of optically active compounds.[1] The asymmetric reduction of prochiral ketones to yield optically pure alcohols can be achieved with metal-based catalysts,[2] but also with enzymes such as alcohol dehydrogenases (ADH). Many studies have been reported in the literature showing the importance of ADH in asymmetric synthesis,[3–5] of relevance is their usually high thermostability,[6,7] and the ability to operate in non-aqueous media with high activity and selectivity.[8,9]

ADH enzymes catalyse the reversible reduction of prochiral ketones to their corresponding alcohols. They require the presence of NAD(P)H as a cofactor, which delivers its *pro*-(R) hydride to the usually *Re* face of the ketone yielding the corresponding (S)-alcohols (see Scheme 1). The stereoselectivity of ADHs towards the formation of (S)-alcohols mainly arises from the shape of the active site of the enzymes that usually present a small and a large binding pocket (see Fig. 1).[10] As most ADH follow Prelog's rule (Scheme 1), the engineering of their active sites for the formation of the (R)-enantiomer, *i.e.* anti-Prelog ADHs, is of great interest. In addition to that, the expansion of the substrate scope of ADH is also highly appealing for broadening their applicability in asymmetric synthesis. To that end, Directed Evolution (DE)[1,11–14] and rational site-specific mutagenesis[15] have been applied in some ADH enzymes. Reetz *et al.* developed a powerful strategy for reducing the number of variants to screen by generating a collection of small but 'smart' enzyme libraries.[16] This was applied on the zinc-depen-

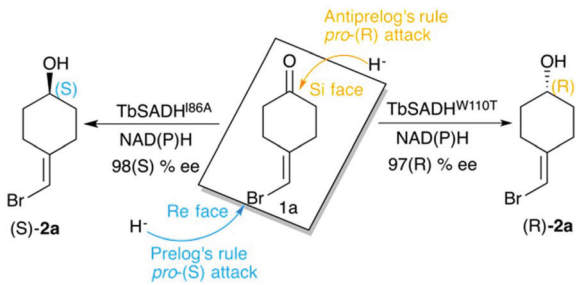

Scheme 1 Representation of Prelog and anti-Prelog rules for the studied substrate **1a**, together with the stereoselectivity of the engineered variants TbSADH^{I86A}, and TbSADH^{W110T} by Reetz *et al.*[20]

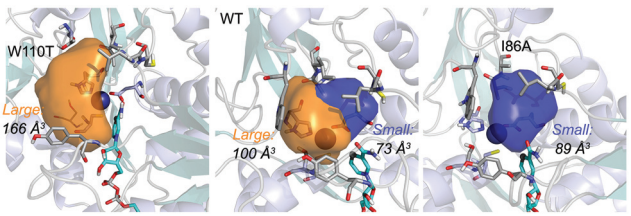

Fig. 1 Volume representation of the small and large TbSADH binding pockets for the WT enzyme (middle), W110T (left), and I86A (right) variants. These calculations have been performed with POVME 2.0.[31]

Institut de Química Computacional i Catàlisi (IQCC) and Departament de Quimica, Universitat de Girona, Carrer Maria Aurèlia Capmany 6, 17003 Girona, Spain. E-mail: silvia.osuna@udg.edu

†Electronic supplementary information (ESI) available. See DOI: 10.1039/C7OB00482F

dent secondary ADH from *Thermoanaerobacter brockii* (TbSADH) for the asymmetric reduction of tetrahydrofuran-3-one towards the (S)-alcohol, which is of importance for the synthesis of the HIV inhibitors amprenavir and fosamprenavir.[16,17] Engineered variants of *Lactobacillus kefir* short-chain alcohol dehydrogenase were also developed for the asymmetric reduction of the same tetrahydrofuran-3-one, but also for the related thiolan-3-one.[18] Phillips and coworkers engineered TbSADH for accepting several structurally diverse ketones.[19] Similarly, Reetz evolved the same ADH for accepting a set of non-cyclic ketones.[6] They also engineered TbSADH for the catalytic asymmetric reduction of prochiral ketones of type 4-alkylidene cyclohexanone with formation of the corresponding axially chiral (R) or (S)-alcohols.[20] Interestingly, the singly mutated variants TbSADH^{W110T} and TbSADH^{I86A} were found to yield respectively either the unusual (R)-alcohol or the (S)-alcohol with high conversion rates and selectivity. The same W110 and I86 positions were found to be important in determining the enantioselectivity of the highly homologous secondary ADH from *Thermoanaerobacter ethanolicus* (TeSADH) enzyme.[8,21–23]

The previously mentioned examples highlight the outstanding performance of laboratory-evolution for enhancing activity, and reversing the enantioselectivity of ADHs. Complementary to experimental evolution, computational methods can be used for rationalizing the activity and selectivity of natural and laboratory-engineered enzymes.[24] Bocola and coworkers elucidated through Quantum Mechanics and Molecular Mechanics (*i.e.* QM/MM) calculations the mechanism of hydride and proton transfer of the oxidoreductase from *Candida Parapsilosis*.[25] Electronic structure calculations and Molecular Dynamics (MD) simulations were performed to investigate the mechanism of liver alcohol dehydrogenase (LADH).[26] The calculations revealed a lower activation barrier for the hydride transfer step if alcohol deprotonation occurs first. Many computational studies have been devoted to elucidate the fundamental nature of hydrogen tunnelling that occurs in these NAD(P)H-dependent enzymes.[27–29] Some of us explored through MD simulations of the Michaelis–Menten and transition state-bound complexes the stereoselectivity of some *Lactobacillus kefir* short-chain alcohol dehydrogenases.[18] These simulations allow rationalising the effect of active site mutations on the selectivity of this Zn(II) free ADH enzyme.

In this study we computationally evaluate the effect of W110 and I86A active site mutations on a series of zinc-dependent TbSADH variants[20] through MD simulations. We demonstrate that the introduced mutations induce dramatic changes in the shape of the enzyme active site, which affect the substrate–enzyme interactions thus determining the stereoselectivity of the TbSADH variants.

2. Results and discussion

ADH enzymes present two differently shaped active site pockets, which are responsible for their substrate scope and selectivities (see Fig. 1). By introducing mutations to the ADH active site, both *pro*-(R) and *pro*-(S) selectivities can be obtained. In most experimental studies based on TbSADH and the homologous TeSADH published so far two positions, namely I86 and W110, have been found to be key for either enhancing the enzyme activity towards bulky substrates and/or reverting the stereoselectivity of ADHs.[9,20,21,23,30] In order to shed some light into the role of the latter mutations in ADH catalytic activity and selectivity, we performed MD simulations on the Wild-Type (WT) TbSADH enzyme, and the variants TbSADH^{W110T} and TbSADH^{I86A}. We restricted our study to the analysis of the prochiral ketone of type 4-alkelidene cyclohexanone (**1a**, see Scheme 1) studied by Reetz and coworkers.[20] This ketone is especially challenging as the steric preferences of the carbon atoms surrounding the carbonyl group are identical. Of importance is the fact that positions I86 and W110 are key to revert the enzyme enantioselectivity even with this non-conventional substrate.

We carried out five independent 200 ns MD simulations (*i.e.* accumulated simulation time of 1 microsecond) in both *pro*-(R) and *pro*-(S) conformations of **1a** in the WT TbSADH, TbSADH^{W110T}, and TbSADH^{I86A} enzyme variants. In order to maintain the substrate **1a** bound to the Zn(II) metal ion, a force constant was applied. This approach allows us to analyse the positioning of **1a** for efficient hydride transfer, and thus explain the activity and origin of enantioselectivity observed experimentally.

As shown in Scheme 1, **1a** has a bromide atom that can be differently oriented in the small and large binding pockets depending on the variant and the starting pose (*pro*-(R) and *pro*-(S) conformation, see Fig. 2–5). The positioning of both the

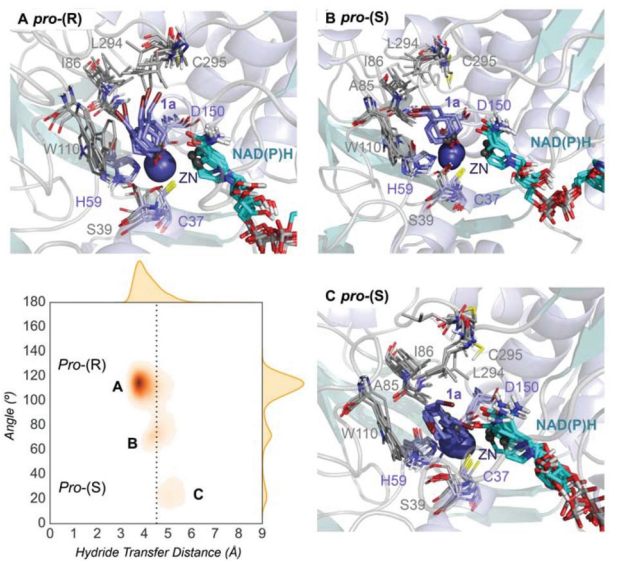

Fig. 2 Representation of some representative snapshots of the different conformational states sampled along the MD simulations for TbSADH starting from the *pro*-(R) orientation of **1a**. The histogram of the hydride transfer distance together with the *pro*-(R)/*pro*-(S) angle (detailed in Fig. S1†) is displayed.

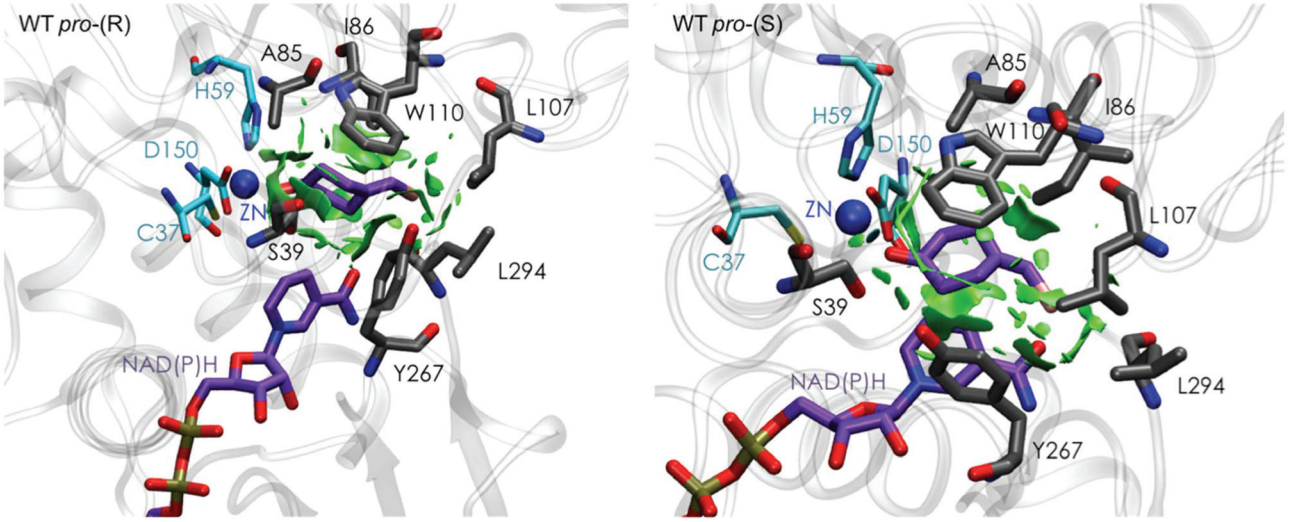

Fig. 3 Representation of the non-covalent interactions for the *pro*-(S) and *pro*-(R) conformations of **1a** in the active site pocket of TbSADH enzyme, computed with the computational tool NCIplot.[34,35]

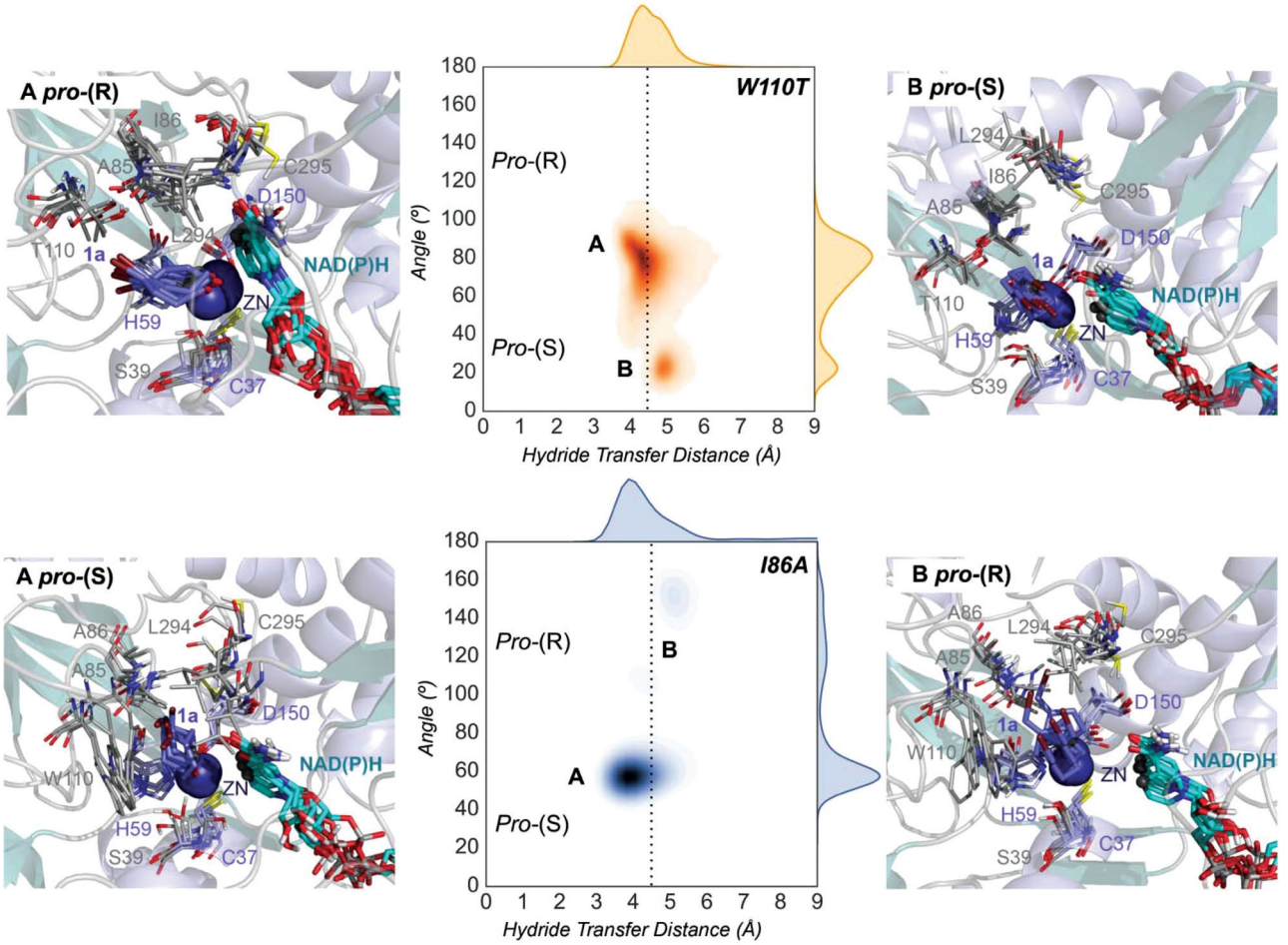

Fig. 4 Representation of some representative snapshots of the different conformational states sampled along the MD simulations for the TbSADH^{W110T} and TbSADH^{I86A} starting from the *pro*-(R) (in orange) and *pro*-(S) (in blue) orientations of **1a**, respectively. The histogram of the hydride transfer distance together with the *pro*-(R)/*pro*-(S) angle (detailed in Fig. S1†) is displayed for both variants.

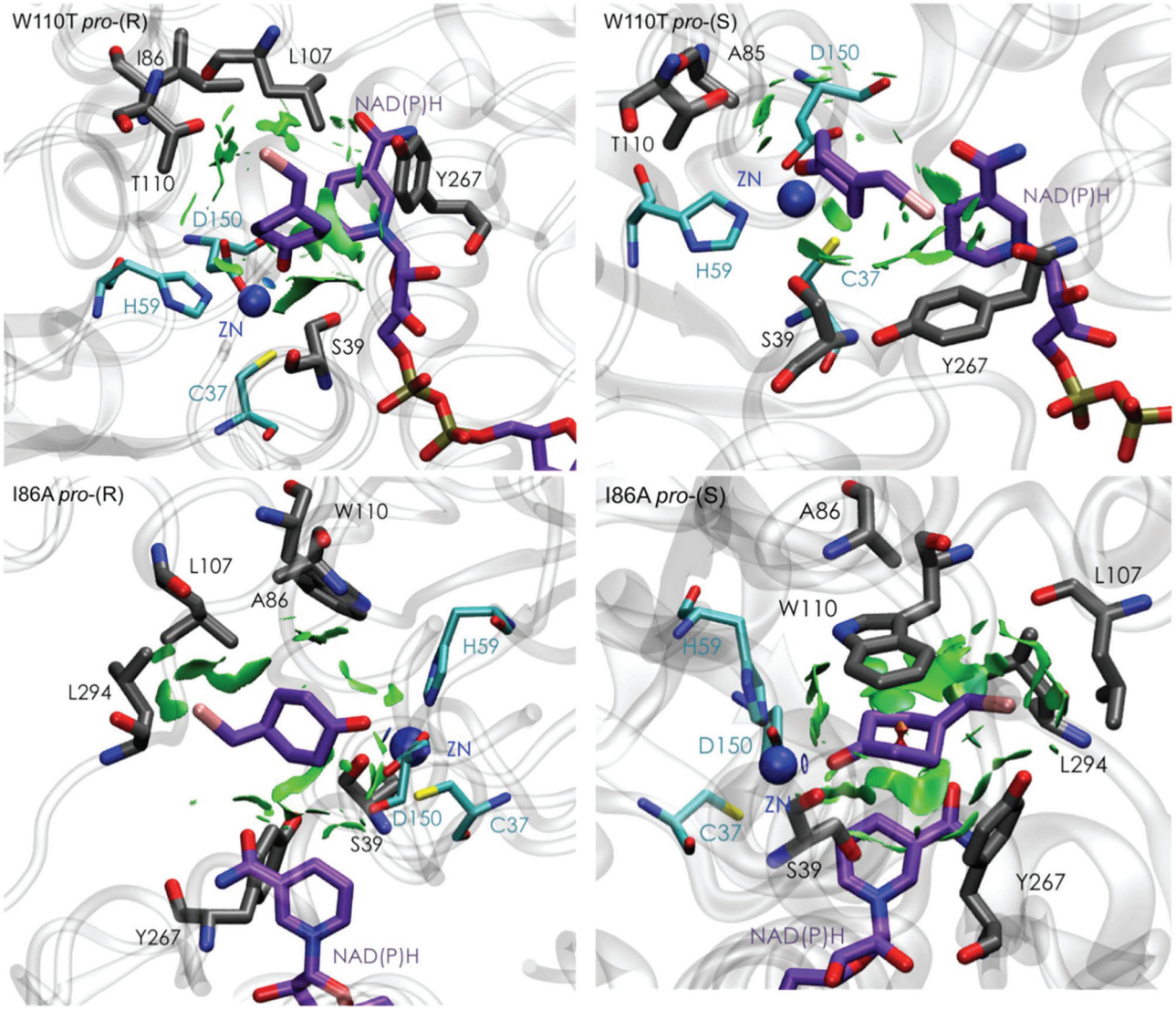

Fig. 5 Representation of the non-covalent interactions for *pro*-(S) and *pro*-(R) conformations of **1a** in the active site pocket of TbSADH^{W110T} (top) and TbSADH^{I86A} (down) enzymes, computed with the computational tool NCIplot.[34,35]

bromide and the cyclohexane ring of **1a** and its interactions with the enzyme active site pocket will dictate ADH selectivity. The difference in activity can be predicted by analysing the distance between the carbonyl group of the substrate and the NAD(P)H carbon atom involved in the hydride transfer (see Scheme 2). Our computed hydride transfer Transition State (TS) using DFT and a small subset of the enzyme active site residues, *i.e.* following the *theozyme* approach,[32] indicates that at the TS it is *ca.* 2.7 Å for both axial and equatorial attacks (see Scheme 2, and Fig. S8†). This is in line with previous calculations for the hydride transfer. As with classical MD simulations we cannot model the bond-breaking/forming hydride transfer step, we instead evaluate the active site preorganization towards the *pro*-(S)/*pro*-(R) enzyme–substrate complexes to shed some light into the enzyme enantioselectivities. We define as catalytically competent poses those MD conformations that present hydride transfer distances shorter than 4.5 Å, whereas those orientations with longer hydride distances were defined as non-catalytic. This allows us to indirectly quantify the number of reactive events along the simulation time, *i.e.* it provides an estimate of the enzyme catalytic activity.

We evaluate ADH enantioselectivity preferences by comparing the angle formed between the carbonyl group of the active site residue T38 (situated next to C37, one of the Zn(II)-coordinating residues), the C5 and C3 carbon of **1a** cyclohexane ring (see Fig. S1†) in all variants. As the NAD(P)H cofactor is in some cases displaced from the active site, the angle provided by the rigid T38 residue together with the measure of the hydride transfer distance allow us to better evaluate the catalytically competent *pro*-(S) and *pro*-(R) conformations. As done in previous studies,[18] by computing the relative populations of

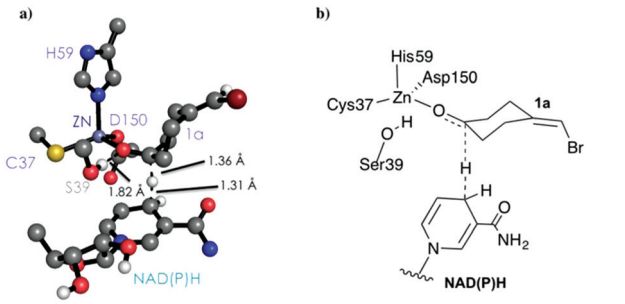

Scheme 2 DFT optimized TS structure for the hydride transfer step. For visualization purposes, non-polar hydrogen atoms are hidden.

the reactive *pro*-(S) and *pro*-(R) poses observed along the MD simulations, the experimental enantiomeric excess ratios can be estimated (see Table S2†).

Evaluation of the TbSADH WT enzyme stereoselectivity

Our analysis starts with the evaluation of the WT TbSADH enzyme activity and selectivity towards **1a**. Reetz *et al.* reported that TbSADH is able to produce the corresponding (R)-alcohol in a 95% conversion, but only with 66 (R) % ee.[20] We evaluated the WT enzyme active site pockets in the most populated conformational states (*i.e.* most visited along the MD simulations) using the computational tool POVME,[31] indicating that the small and large active site pockets have an approximated volume of *ca.* 73 Å^3 and 100 Å^3 (see Fig. 1 and Table S1†), which evidence their drastic difference in size as observed with X-ray structures.[33]

In our TbSADH MD simulations starting from the *pro*-(R) orientation of **1a**, the bromide atom is forced to fit in the small pocket because the bulky W110 residue does not allow the rotation of the substrate towards the large binding pocket (see Fig. 2, *pro*-(R) A). This corresponds to the most populated conformation, where **1a** remains properly positioned for the hydride transfer to occur towards its Si-face and thus allowing the (R)-alcohol formation. The average hydride distance is *ca.* 3.9 Å, which coincides with the computed hydride transfer distance at the reactant complex (*i.e.* 3.8 Å).[27] This rather short distance is in agreement with the high conversion rate observed experimentally. The analysis of non-covalent interactions with the NCI plot of **1a** in the *pro*-(R) conformation reveals stabilizing C–H···π interactions between H59, Y267, and W110 with the cyclohexane ring of the substrate (see Fig. 3). In contrast, the latter stabilizing interactions are much weaker in the *pro*-(S) conformations (in particular non-covalent interactions with the residue W110), which evidence how the TbSADH pocket is more complementary to the *pro*-(R) conformation of **1a** to produce the corresponding (R)-alcohol.

In the MD simulations starting from the *pro*-(S) conformation of **1a**, short catalytic distances of *ca.* 3.9 Å are also observed (see Fig. S2 A†), where **1a** is properly positioned for the formation of the (S)-alcohol. However, this *pro*-(S) catalytically active conformation has a quite low population. This rather low stability of the *pro*-(S) conformation is also evidenced by analysing the non-covalent interactions of **1a** and the active site pocket of TbSADH. The enzyme also adopts some intermediate conformations that present substantially longer unproductive hydride transfer distances. Overall, our MD simulations on TbSADH starting from both *pro*-(R) and *pro*-(S) orientations of **1a** indicate that the formation of the (R)-alcohol is substantially preferred, although some catalytically competent *pro*-(S) conformations are also explored. This is in line with the 66% (R) ee observed in the experimental assays.

Evaluation of the TbSADH^{W110T} and TbSADH^{I86A} enzyme stereoselectivity

The substitution of W110 by threonine makes the enzyme large binding pocket even wider. The computed volume is *ca.* 166 Å^3, whereas for the TbSADH it was 100 Å^3 (as discussed previously). This mutation therefore gives extra space to **1a** for a better accommodation of the bromide substituent in the enzyme active site pocket, and thus allows the substrate to rotate towards the large binding site. Experimentally, it was found that TbSADH^{W110T} was able to convert **1a** into the corresponding (R)-alcohol with high conversion rates and high enantioselectivities (99% conversion, and 97 (R) % ee).[20] In this enzyme variant, angles of *ca*. 70° are observed for the *pro*-(R) conformation, whereas *ca.* 20° for the *pro*-(S) attack (see Fig. 4, W110T A and B).

In our MD simulations starting from the *pro*-(R) orientation of **1a**, the substrate rapidly rotates to position the bromide into the large binding pocket, and remains in this *pro*-(R) orientation most of the simulation time (see Fig. 4, W110T). The NAD(P)H cofactor is perfectly positioned to deliver the hydride and allow the (R)-alcohol formation (see Fig. 4, W110T *pro*-(R) A) displaying catalytically competent hydride distances and angles. Moreover, starting from *pro*-(S) orientations (Fig. S3†) **1a** rapidly rotates towards pro-(R) conformations.

The analysis of non-covalent interactions in the *pro*-(R) conformations of **1a** reveals stabilizing C–H···π interactions between the cyclohexane ring of the substrate and residues H59, and Y267, but also with the nicotinamide ring of the NAD(P)H cofactor (see Fig. 5, W110T *pro*-(R)). The W110T mutation enlarges the active site pocket, but also allows the formation of stabilizing interactions between the bromide and the side-chains of L107 and the newly introduced T110 residue. We also observe during the MD simulations that the substrate can rotate to explore *pro*-(S) conformations (see Fig. 4, W110T *pro*-(S) B), however long hydride distances are observed due to the displacement of the NADP(H) cofactor, which interacts with the bromide atom of the substrate (see Fig. 5, W110T *pro*-(S)).

We finally evaluated the TbSADH^{I86A} enzyme variant, which was found to allow the formation of the opposite (S)-alcohol in high enantiomeric excess (98 (S) % ee), and conversion (95%). Our volume calculations on the most populated conformational states indicate that the small enzyme active site pocket is enlarged from *ca.* 73 to 89 Å^3. In contrast to what we observe in the TbSADH and TbSADH^{W110T} variants, MD simulations

starting from the *pro*-(S) poses of **1a** reveal that the substrate stays in the *pro*-(S) conformations with an angle of *ca.* 60° most of the simulation time (see Fig. 4, I86A *pro*-(S) A). In this most populated state, catalytically competent hydride transfer distances are sampled (*ca.* 4 Å), which fits with the high activity of the variant observed experimentally. This favourable *pro*-(S) conformations are mainly stabilized by C–H···π interactions between the cyclohexane ring and residues W110, H59, and Y267 (see Fig. 5, I86A *pro*-(S)). As observed in the case of $TbSADH^{W110T}$, C–H···π interactions are also observed within the cyclohexane ring and the nicotinamide ring of NAD(P)H. The mutation introduced at position 86 (*i.e.* I86A) creates additional space in the small binding pocket, which is occupied by the indole ring of W110. This new conformation of W110 maximizes the C–H···π interactions with the cyclohexane ring of **1a**, and thus favors the *pro*-(S) attack (see Fig. 5, I86A *pro*-(S)).

In the MD simulations, when **1a** rotates to explore *pro*-(R) conformations, long hydride transfer distances are observed due to the displacement of the NAD(P)H cofactor (see Fig. 4, I86A *pro*-(R) B). MD simulations starting from the *pro*-(R) conformation (Fig. S4†) show that the substrate stays most of the time in the *pro*-(R) orientation, but again leads to the displacement of the NAD(P)H cofactor and thus results in a non-catalytic configuration. The analysis of non-covalent interactions in this *pro*-(R) conformation reveals that most of the above mentioned interactions with W110, H59, and Y267 are lost (see Fig. 5, I86A *pro*-(R)). These results point out that although **1a** can adopt both *pro*-(R) and *pro*-(S) orientations, *pro*-(S) is the catalytically competent pose as only with this orientation both **1a** and NAD(P)H are properly positioned for the catalysis.

3. Conclusions

Our MD simulations indicate that the poor selectivity of the WT TbSADH enzyme is due to the possible positioning of the substrate in both *pro*-(R) and *pro*-(S) orientations. The *pro*-(R) conformation is, however, substantially favoured due to stronger non-covalent interactions between the substrate and the enzyme active site. $TbSADH^{W110T}$ presents a substantially wider active site, especially the large binding pocket, which allows the substrate to explore *pro*-(R) conformations with catalytically active hydride transfer distances. In the *pro*-(R) conformation, C–H···π interactions are observed between the cyclohexane ring and active site residues H59 and Y267. The introduced threonine residue at position 110 also allows the formation of stabilizing interactions between its side-chain and the bromide group of **1a**. $TbSADH^{I86A}$ enzyme variant shows a significantly different behaviour revealing a highly pre-organized active site for the *pro*-(S) conformation with catalytically efficient distances. The introduced I86A mutation enlarges the small binding pocket, and induces a conformational change in W110 that optimally positions the indole group for enhanced C–H···π interactions with the cyclohexane ring of the substrate. The combination of MD simulations, *theozyme* calculations, and in-depth analysis of the active site pocket through the computational tools POVME and NCIplot allows us to rationalise the effect of these two key active site mutations in the enantioselectivity of the zinc-dependent TbSADH enzyme. Given that many studies based on TbSADH and TeSADH target the same active site mutations, we believe that the obtained results are rather general. Our results also highlight the feasibility of MD simulations, coupled with POVME and NCIplot calculations for the engineering of natural enzyme active sites for enhanced activity and selectivity.

Computational methods

MD simulations in explicit water were performed using AMBER 16 package[4] and starting from the PDB structure: 1YKF.[33] The W110T and I86A variants were generated using the mutagenesis tool included in PyMOL (http://www.pymol.org). Parameters for substrate **1a** for the MD simulations were generated within the *antechamber* module of AMBER 16 using the general AMBER force field (GAFF),[36] with partial charges set to fit the electrostatic potential generated at the B3LYP/6-31G(d) level by the restrained electrostatic potential (RESP) model.[37] The charges were calculated according to the Merz–Singh–Kollman scheme[38,39] using Gaussian 09.[40] Amino acid protonation states were predicted using the H++ server (http://biophysics.cs.vt.edu/H++).[41] We have used the bonded model for Zn and the residues of the first coordination sphere, in particular we used the Seminario approach[42] to obtain the metal parameters needed for the simulation as implemented in Prof. Ryde program.[43] The optimization, frequencies and charge calculations to obtain the parameters were done at the B3LYP/6-31G(d) level using Gaussian 09.[40] The parameters for NAD(P)H were extracted from previous studies by Prof. Ryde.[44,45] The WT enzyme (PDB: 1YKF) and variant were solvated in a pre-equilibrated truncated cuboid box with a 10 Å buffer of TIP3P[46] water molecules using the AMBER16 *leap* module, resulting in the addition of *ca.* 11 000 solvent molecules. The system was neutralized by the addition of explicit counterions (Na^+ and Cl^-). All calculations were done using the *ff*14SB Amber force field.[47] A two-stage geometry optimization approach was performed. The first stage minimizes the positions of solvent molecules and ions imposing positional restraints on the solute by a harmonic potential with a force constant of 500 kcal mol^{-1} $Å^{-2}$, and the second stage is an unrestrained minimization of all the atoms in the simulation cell. The systems are gently heated using six 50 ps steps, incrementing the temperature 50 K each step (0–300 K) under constant volume and periodic boundary conditions. Water molecules were treated with the SHAKE algorithm such that the angle between the hydrogen atoms is kept fixed. Long-range electrostatic effects were modeled using the particle-mesh-Ewald method.[48] An 8 Å cutoff was applied to Lennard-Jones and electrostatic interactions. Harmonic restraints of 10 kcal mol^{-1} were applied to the solute, and the Langevin equilibration scheme was used to control and equalize the temperature. The time step was maintained at 1 fs during the heating stages, allowing potential inhomogeneities to self-adjust. Each

system was then equilibrated without restrains for 2 ns with a 2 fs time step at a constant pressure of 1 atm and a temperature of 300 K. After the systems were equilibrated in the NPT ensemble, 3 independent five hundred nanosecond MD simulations were performed under the NVT ensemble and periodic-boundary conditions.

The *theozyme* calculations for the hydride transfer step were performed at the B3LYP/6-31G(d) level of theory using Gaussian 09.[40] Active site volume calculations were performed with the computational tool POVME 2.0.[31]

Acknowledgements

A. R. R. thanks the Generalitat de Catalunya for a PhD fellowship (2015-FI-B-00165), M. A. M. S. is grateful to the Spanish MINECO for a PhD fellowship (BES-2015-074964). S. O. thanks the Spanish MINECO for project CTQ2014-59212-P, Ramón y Cajal contract (RYC-2014-16846), the European Community for CIG project (PCIG14-GA-2013-630978), and the funding from the European Research Council (ERC) under the European Union's Horizon 2020 research and innovation programme (ERC-2015-StG-679001). We are grateful for the computer resources, technical expertise, and assistance provided by the Barcelona Supercomputing Center – Centro Nacional de Supercomputacion.

Notes and references

1 U. T. Bornscheuer, G. W. Huisman, R. J. Kazlauskas, S. Lutz, J. C. Moore and K. Robins, *Nature*, 2012, **485**, 185–194.
2 R. H. Morris, *Chem. Soc. Rev.*, 2009, **38**, 2282–2291.
3 E. García-urdiales, I. Alfonso and V. Gotor, *Chem. Rev.*, 2005, **105**, 313–354.
4 W. Kroutil, H. Mang, K. Edegger and K. Faber, *Curr. Opin. Chem. Biol.*, 2004, **8**, 120–126.
5 Y.-G. Zheng, H.-H. Yin, D.-F. Yu, X. Chen, X.-L. Tang, X.-J. Zhang, Y.-P. Xue, Y.-J. Wang and Z.-Q. Liu, *Appl. Microbiol. Biotechnol.*, 2017, **101**, 987–1001.
6 Z. Sun, G. Li, A. Ilie and M. T. Reetz, *Tetrahedron Lett.*, 2016, **57**, 3648–3651.
7 D. S. Burdette, V. Tchernajencko and J. G. Zeikus, *Enzyme Microb. Technol.*, 2000, **27**, 11–18.
8 M. M. Musa, K. I. Ziegelmann-fjeld, C. Vieille, J. G. Zeikus and R. S. Phillips, *Angew. Chem., Int. Ed.*, 2007, **46**, 3091–3094.
9 M. M. Musa, K. I. Ziegelmann-fjeld, C. Vieille and R. S. Phillips, *Org. Biomol. Chem.*, 2008, **6**, 887–892.
10 V. Prelog, in *Pure Appl. Chem*, 1964, vol. 9, p. 119.
11 A. S. Bommarius, *Annu. Rev. Chem. Biomol. Eng.*, 2015, **6**, 319–345.
12 M. T. Reetz, *Directed Evolution of Selective enzymes: Catalysts for Organic Chemistry and Biotechnology*, Wiley-VCH, Weinheim, 2016.
13 A. Currin, N. Swainston, P. J. Day and D. B. Kell, *Chem. Soc. Rev.*, 2015, **44**, 1172–1239.
14 S. Lutz and U. T. Bornscheuer, *Protein Engineering Handbook*, Wiley-VCH Verlag GmbH & Co. KGaA, 2008.
15 J. Pleiss, in *Enzyme Catalysis in Organic Synthesis*, Wiley-VCH Verlag GmbH & Co. KGaA, 2012, pp. 89–117.
16 Z. Sun, R. Lonsdale, A. Ilie, G. Li, J. Zhou and M. T. Reetz, *ACS Catal.*, 2016, **6**, 1598–1605.
17 A. Nobili, M. G. Gall, I. V. Pavlidis, M. L. Thompson, M. Schmidt and U. T. Bornscheuer, *FEBS J.*, 2013, **280**, 3084–3093.
18 E. L. Noey, N. Tibrewal, G. Jiménez-osés, S. Osuna, J. Park, C. M. Bond, D. Cascio, J. Liang, X. Zhang, G. W. Huisman, Y. Tang and K. N. Houk, *Proc. Natl. Acad. Sci. U. S. A.*, 2015, **112**, E7065–E7072.
19 C. M. Nealon, M. M. Musa, J. M. Patel and R. S. Phillips, *ACS Catal.*, 2015, **5**, 2100–2114.
20 R. Agudo, G.-D. Roiban and M. T. Reetz, *J. Am. Chem. Soc.*, 2012, **135**, 1665–1668.
21 M. M. Musa, N. Lott, M. Laivenieks, L. Watanabe, C. Vieille and R. S. Phillips, *ChemCatChem*, 2009, **1**, 89–93.
22 K. I. Ziegelmann-fjeld, M. M. Musa, R. S. Phillips, J. G. Zeikus and C. Vieille, *Protein Eng., Des. Sel.*, 2007, **20**, 47–55.
23 M. M. Musa, K. I. Ziegelmann-fjeld, C. Vieille, J. G. Zeikus and R. S. Phillips, *J. Org. Chem.*, 2007, **72**, 30–34.
24 A. Romero-rivera, M. Garcia-borras and S. Osuna, *Chem. Commun.*, 2017, **53**, 284–297.
25 G. V. Dhoke, M. D. Davari, U. Schwaneberg and M. Bocola, *ACS Catal.*, 2015, **5**, 3207–3215.
26 P. K. Agarwal, S. P. Webb and S. Hammes-schiffer, *J. Am. Chem. Soc.*, 2000, **122**, 4803–4812.
27 D. Roston and A. Kohen, *Proc. Natl. Acad. Sci. U. S. A.*, 2010, **107**, 9572–9577.
28 S. R. Billeter, S. P. Webb, P. K. Agarwal, T. Iordanov and S. Hammes-schiffer, *J. Am. Chem. Soc.*, 2001, **123**, 11262–11272.
29 D. Roston and A. Kohen, *J. Am. Chem. Soc.*, 2013, **135**, 13624–13627.
30 M. M. Musa, J. M. Patel, C. M. Nealon, C. S. Kim, R. S. Phillips and I. Karume, *J. Mol. Catal. B: Enzym.*, 2015, **115**, 155–159.
31 J. D. Durrant, L. Votapka, J. Sørensen and R. E. Amaro, *J. Chem. Theory Comput.*, 2014, **10**, 5047–5056.
32 D. J. Tantillo, C. Jiangang and K. N. Houk, *Curr. Opin. Chem. Biol.*, 1998, **2**, 743–750.
33 Y. Korkhin, A. J. Kalb, M. Peretz, O. Bogin, Y. Burstein and F. Frolow, *J. Mol. Biol.*, 1998, **278**, 967–981.
34 J. Contreras-García, E. R. Johnson, S. Keinan, R. Chaudret, J.-P. Piquemal, D. N. Beratan and W. Yang, *J. Chem. Theory Comput.*, 2011, **7**, 625–632.
35 E. R. Johnson, S. Keinan, P. Mori-Sánchez, J. Contreras-garcía, A. J. Cohen and W. Yang, *J. Am. Chem. Soc.*, 2010, **132**, 6498–6506.
36 J. Wang, R. M. Wolf, J. W. Caldwell, P. A. Kollman and D. A. Case, *J. Comput. Chem.*, 2004, **25**, 1157–1174.

37 C. I. Bayly, P. Cieplak, W. Cornell and P. A. Kollman, *J. Phys. Chem.*, 1993, **97**, 10269–10280.
38 U. C. Singh and P. A. Kollman, *J. Comput. Chem.*, 1984, **5**, 129–145.
39 B. H. Besler, K. M. Merz and P. A. Kollman, *J. Comput. Chem.*, 1990, **11**, 431–439.
40 M. J. Frisch, G. W. Trucks, H. B. Schlegel, G. E. Scuseria, M. A. Robb, J. R. Cheeseman, G. Scalmani, V. Barone, G. A. Petersson, H. Nakatsuji, X. Li, M. Caricato, A. Marenich, J. Bloino, B. G. Janesko, R. Gomperts, B. Mennucci, H. P. Hratchian, J. V. Ortiz, A. F. Izmaylov, J. L. Sonnenberg, D. Williams-young, F. Ding, F. Lipparini, F. Egidi, J. Goings, B. Peng, A. Petrone, T. Henderson, D. Ranasinghe, V. G. Zakrzewski, J. Gao, N. Rega, G. Zheng, W. Liang, M. Hada, M. Ehara, K. Toyota, R. Fukuda, J. Hasegawa, M. Ishida, T. Nakajima, Y. Honda, O. Kitao, H. Nakai, T. Vreven, K. Throssell, J. A. Montgomery Jr., J. E. Peralta, F. Ogliaro, M. Bearpark, J. J. Heyd, E. Brothers, K. N. Kudin, V. N. Staroverov, T. Keith, R. Kobayashi, J. Normand, K. Raghavachari, A. Rendell, J. C. Burant, S. S. Iyengar, J. Tomasi, M. Cossi, J. M. Millam, M. Klene, C. Adamo, R. Cammi, J. W. Ochterski, R. L. Martin, K. Morokuma, O. Farkas, J. B. Foresman and D. J. Fox, *Gaussian 09, Revision D.01*, Gaussian Inc., Wallingford, CT, 2009.
41 R. Anandakrishnan, B. Aguilar and A. V. Onufriev, *Nucleic Acids Res.*, 2012, **40**, W537–W541.
42 J. M. Seminario, *Int. J. Quantum Chem.*, 1996, **60**, 1271–1277.
43 L. Hu and U. Ryde, *J. Chem. Theory Comput.*, 2011, **7**, 2452–2463.
44 U. Ryde, *Proteins*, 1995, **21**, 40–56.
45 U. Ryde, *Protein Sci.*, 1995, **4**, 1124–1132.
46 W. L. Jorgensen, J. Chandrasekhar, J. D. Madura, R. W. Impey and M. L. Klein, *J. Chem. Phys.*, 1983, **79**, 926–935.
47 V. Hornak, R. Abel, A. Okur, B. Strockbine, A. Roitberg and C. Simmerling, *Proteins*, 2006, **65**, 712–725.
48 T. Darden, D. York and L. Pedersen, *J. Chem. Phys.*, 1993, **98**, 10089–10092.